The Astrophysical Journal Letters, 921:L32 (8pp), 2021 November 10 https://doi.org/10.3847/2041-8213/ac31aa
© 2021. The Author(s). Published by the American Astronomical Society.
OPEN ACCESS

X-Ray Quasi-periodic Eruptions Driven by Star–Disk Collisions: Application to GSN069 and Probing the Spin of Massive Black Holes

Jingtao Xian[1], Fupeng Zhang[1,2,3], Liming Dou[1,2,3], Jiasheng He[1], and Xinwen Shu[4]
[1] School of Physics and Materials Science, Guangzhou University, Guangzhou 510006, People's Republic of China; zhangfupeng@gzhu.edu.cn
[2] Key Laboratory for Astronomical Observation and Technology of Guangzhou, Guangzhou 510006, People's Republic of China
[3] Astronomy Science and Technology Research Laboratory of Department of Education of Guangdong Province, Guangzhou 510006, People's Republic of China
[4] Department of Physics, Anhui Normal University, Wuhu, Anhui 241002, People's Republic of China
Received 2021 September 12; revised 2021 October 18; accepted 2021 October 20; published 2021 November 5

Abstract

X-ray quasi-periodic eruptions (QPEs) were discovered recently in active galaxies with an unknown driving mechanism. Under the assumption that QPEs are caused by star–disk collisions, we adopt full relativistic method and show that both the orbital parameters of the star and also the mass and spinning of the massive black hole (MBH) can be revealed by using the time of arrival (TOA) of the QPEs. By applying the model to the observed QPEs of GSN069, we find that the star is in a near-circular orbit ($e_\star = 0.05^{+0.02}_{-0.02}$) with a semimajor axis of $\sim 365^{+54}_{-49} r_g$ around an MBH with $M_\bullet = 3.0^{+0.9}_{-0.6} \times 10^5\, M_\odot$. The alternative short and long recurring time of the QPEs of GSN069 can be well explained by the small eccentricity and the orbital precession of the star. We find that the QPEs of GSN069 are possibly driven by a striped stellar core colliding with accretion disk after a partial tidal disruption event around the MBH. For GSN069-like galaxies, if continuous X-ray monitoring of QPE events can be accumulated with uncertainties of TOA $\lesssim$100–150 s, the spin of the MBH can be constrained by fitting to QPEs. Our results show that the timing of QPEs can provide a unique probe for measuring the spinning of the MBH and tests of the no-hair theorem.

Unified Astronomy Thesaurus concepts: Tidal disruption (1696); X-ray bursts (1814); Supermassive black holes (1663); General relativity (641); Kerr black holes (886)

1. Introduction

X-ray quasi-periodic eruptions (QPEs) are rapid and extremely intensive bursts of X-ray emission that repeat about every few hours from regions around massive black holes (MBHs) in galactic nuclei. QPEs have been found recently from the active galactic nucleus of GSN069 (Miniutti et al. 2019) and galaxy J1301.9+2747 (Giustini et al. 2020). More recently, QPEs are detected in the nucleus of two previously quiescent galaxies (Arcodia et al. 2021). Multiple epochs of observations suggest that QPEs may last from at least months to decades (Miniutti et al. 2019; Giustini et al. 2020). Currently the underlying physical mechanism that drives the bursts of these events is still unclear. Some of the possibilities are the limit-cycle oscillations induced by instabilities of the accretion flow (Lightman & Eardley 1974) or an edge-on binary black hole gravitationally lensing the light from each others' accretion disk (AD; Ingram et al. 2021). However, they are both found to be inconsistent with the properties of the eruptions (Arcodia et al. 2021). Other possibilities are the falling clumps of a partial tidal disruption event (TDE; Coughlin & Nixon 2020), or the outburst that arose due to the misalignment between the disk and the spin of the MBH (Raj & Nixon 2021). One of the possible mechanisms is that the X-ray QPEs are driven by an orbiter around the MBH that has a mass much smaller than the MBH (Arcodia et al. 2021). One such example is a white dwarf partially disrupted by an MBH when crossing the periapse per orbit (King 2020).

It has been suggested that quasi-periodic flares may be produced by collisions between a star and an accretion disk surrounding an MBH (Karas & Vokrouhlicky 1994; Nayakshin et al. 2004; Dai et al. 2010). Due to collision on the disk, gases are shocked, and subsequently a bright hot spot may appear and evolve on the disk (Zentsova 1983; Ivanov et al. 1998; Semerák et al. 1999; Nayakshin et al. 2004; Pihajoki 2016; Pasham et al. 2019; Suková et al. 2021). The star–disk collision model may be able to explain the X-ray periodicity of galaxy RE J1034+396 (Dai et al. 2010; Gierliński et al. 2008), and the optical variability of source OJ287 (Lehto & Valtonen 1996; Dai et al. 2010). By adopting post-Newtonian methods, Valtonen et al. (2008, 2011) show that the timing of these flares may be a useful probe for general relativity in a strong field.

Here we study the timing of X-ray QPEs under the assumption that they are driven by the star–disk collisions. We use a full general relativistic numerical method (developed in Zhang et al. 2015; Zhang & Saha 2017) to simulate the orbit of a star and also the propagation of lights emitted from the disk to the observer. We then develop a numerical method that can extract the orbital parameters of the star from the timing of X-ray QPEs. We apply the method to GSN069 and set constraints on the orbit of the star. We also discuss the possibility that the orbiter in GSN069 is a result of a partial TDE. We further show that using QPEs alone can set strong constraints on the spinning of the massive black hole if QPEs can be observed with a high enough timing accuracy. Details of the modeling and the results are shown in the following sections.

2. Model and Methodology

The primary assumption is that the X-ray eruptions are due to supersonic collisions between a star[5] bound to the MBH and

Original content from this work may be used under the terms of the Creative Commons Attribution 4.0 licence. Any further distribution of this work must maintain attribution to the author(s) and the title of the work, journal citation and DOI.

[5] We will show later that the orbiter is actually more consistent with a remnant core of a red giant after a partial TDE. Nevertheless, we generally call the orbiter "a star" throughout the Letter.

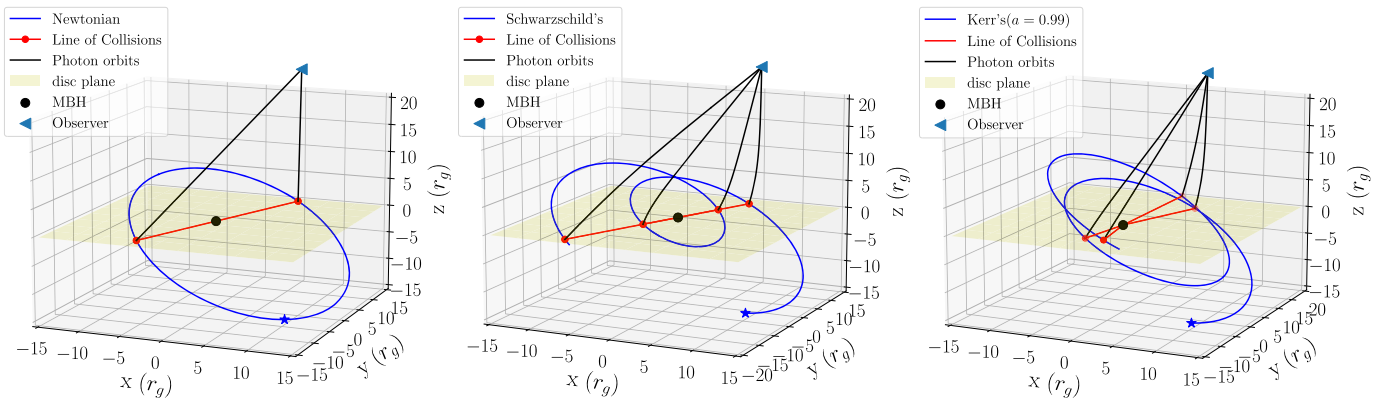

Figure 1. Illustration on the trajectories of the orbiter and the photons in the Newtonian case (left panel) and the relativistic cases for a Schwarzschild MBH (middle panel) and a spinning MBH (right panel). For illustration purposes, the observer is located at distance of $r = 30\ r_g$ from the MBH (for simulations performed in this work, it is actually at $r = 10^7\ r_g$). Note that the ascending node or descending node of the orbiter (the red solid line) remains constant for a Schwarzschild MBH, but change in each revolution for a spinning MBH due to the precession of the orbital plane of the orbiter.

a standard geometrically thin AD, similar to those in Rauch (1995) and Dai et al. (2010). Here we adopt a full general relativistic numerical framework developed in Zhang et al. (2015; see also Zhang & Saha 2017) to calculate the orbit of the star and the propagation of lights from the disk to the observer under Boyer–Lindquist coordinates.

Suppose that the peak of each QPE corresponds to the time when the star intersects with the midplane of the disk. At each time of intersection, we use a ray-tracing technique to trace back a number of photons from a distant observer until we find the one that hits on the position within distance of $<10^{-8} r_\bullet$ from the star, where $r_\bullet$ is the distance of the star to the MBH. The ray tracing is fast and accurate as we use Jacobian elliptic functions and a Gauss–Kronrod integration scheme for the integration of the motion equation of photons (for more details see Zhang et al. 2015).

Then the time of arrival (TOA) $t_{\rm TOA}$ of the eruption due to collision measured in the observer's frame is then given by

$$t_{\rm TOA} = t_\star + t_{\rm prop}, \tag{1}$$

where $t_\star$ is the coordinate time of the star when it intersects with the disk midplane and $t_{\rm prop}$ is the time of propagation of the photon from the intersection to the observer found by the ray-tracing method.

For simplicity, we ignore the secondary image of the eruption produced by photons running around the other side of the MBH and twisting back to the observer, as usually the amplitude of these high-order images is small (Karas & Vokrouhlicky 1994; Dai et al. 2010). We also ignore the gravitational-wave orbital decay and the possible deviations of the star orbit due to collision for now, as we find later that they can be safely ignored for GSN069 (see more details in Section 4).

Figure 1 illustrates examples of trajectories of orbiters and photons in the Newtonian case (left panel) and the relativistic cases under Schwarzschild and spinning MBHs (middle and right panels). We can see that the orbit of the star intersects with the accretion disk twice per orbit, with the time of intersection separating with alternate short and long intervals if there is a nonzero orbital eccentricity. Meanwhile, the orbit of the star is precessing due to relativistic effects (Schwarzschild orbital precession, etc.); thus, the location of the intersection will change in each revolution. Due to the curved spacetime under the Schwarzschild or Kerr metrics, the propagating time of photons from the position of the intersection to the observer is also different. Combining these effects, the TOA of each eruption may then appear with irregular periods.

As the TOA of X-ray QPEs encode various orbital and relativistic effects, in principle the parameters of the MBH or orbit of the star should be reconstructed by the timing of QPEs. We then apply our method to the QPEs observed in GSN069, with more details shown in the following section. As we find that the current observations of GSN069 are not able to recover the spin parameters of the MBH, we discuss the constraints of spin parameters from timing of QPEs for future observations in Section 5.

3. Extracting the Orbit of Star by X-Ray Timing of QPEs in GSN069

Multiple QPEs on Seyfert galaxy GSN069 have been reported by Miniutti et al. (2019), which recur every ∼9 hr with a duration of about ∼1 hr around an MBH of mass $4 \times 10^5\ M_\odot$ according to the timescale (Miniutti et al. 2019). The four epochs of observations collect up to 15 QPEs in a time span of about ∼160 days.

In principle, the MBH–star system contains a total of nine independent parameters: three independent parameters for MBH: mass ($M_\bullet$), the dimensionless magnitude of spin (a), the line-of-sight inclination of spin (i, or the normal direction of the accretion disk if $a = 0$); six parameters of the orbit of star that is defined on the disk plane: the semimajor axis (SMA, $a_\star$), eccentricity ($e_\star$), inclination ($I_\star$), ascending node ($\Omega_\star$, defined with respect to the projection line of sight on the disk plane), argument of periapsis ($\omega_\star$), and the true anomaly ($f_\star$). Parameter $M_\bullet$ can also be replaced by the Keplerian orbital period $P_k = 2\pi (a_\star^3/M_\bullet)^{1/2}$ as $M_\bullet$ can be determined given P_k and $a_\star$.

Due to the limited timing accuracy of each TOA, we found that the spin of MBH cannot be reconstructed for GSN069; thus, we fix $a = 0$. If alternatively we set $a = 0.99$, we find that the constraints on other parameters are only weakly affected. The independent parameters of the model in the case of a Schwarzschild black hole reduce to 6 (Dai et al. 2010): P_k or $M_\bullet$, $a_\star$, $e_\star$, $\alpha_\star$, $\omega_\star$, and $f_\star$, where $\alpha_\star$ is the angle between the vector pointing from the MBH to the ascending node of the star

and the vector pointing from the MBH to the observer, and $\cos\alpha_\bullet = \sin i \cos\Omega_\bullet$.

We then use the Markov Chain Monte Carlo (MCMC) method to reconstruct these parameters. As the observations are on discrete time periods with a different number of eruptions, it is difficult to correspond an eruption in observation to that in simulation. Thus, here we evaluate the χ^2 value by a method similar to those in the pulsar timing. Suppose that there is a sequence of QPEs indexed by $k = 1, 2, \ldots$ and the TOA of the kth one is given by $t_{\mathrm{TOA},k} = \mathcal{F}(k)$. In observation, not all of them are covered. If there are N discrete observations, and the number of QPEs in each one is given by M_i, $i = 1, \ldots, N$, then χ^2 is given by

$$\chi_d^2 = \sum_{i=1}^{N}\sum_{j=1}^{M_i} \frac{(\mathcal{F}^{-1}(t_{\mathrm{TOA},ij}) - (I_{i,j=1} + j - 1))^2}{\sigma_{\mathrm{pij}}^2}, \quad (2)$$

where

$$\sigma_{\mathrm{pij}} = \sigma_{tij} \frac{\partial(\mathcal{F}^{-1})}{\partial t}\bigg|_{t=t_{\mathrm{TOA},ij}},$$

and $\mathcal{F}^{-1}(t_{\mathrm{TOA},ij})$ is the inverse function that connects the TOA of the jth flare of the ith observation to the index k. $I_{j=1}$ is an integer that is closest to the index given by $\mathcal{F}^{-1}(t_{\mathrm{TOA},i1})$. σ_{tij} is the measurement error of the TOA of the jth flare of the ith observation.

Due to the random brightness fluctuations of the QPE events, it is difficult to get directly the peak of each QPE from the observed lightcurves. We adopt the Bayesian block method (Vaughan 2010; Scargle et al. 2013), which can split the time series into optimal segments to help to identify the peak location of each QPE event. The analysis results for the observed QPEs of GSN069 are shown in Figure 2. The TOA of each QPE is reasonably expected to be located at the center of the Bayesian blocks with a maximum flux of a local time series, and the 1σ measurement error of TOA is assumed to be half of the time span of that block. The uncertainty of the TOA for QPEs in GSN069 is found to be between 430–875 s.

The reconstructed parameters are shown in Figure 3 and Table 1. We find that the TOA of QPEs of GSN069 is consistent with an orbiter with an SMA of $\sim$365 r_g and a small eccentricity of $\sim$0.05 (according to the mean likelihood, marked by a light-blue cross in each panel of Figure 3). The angle $\alpha_\bullet \sim 106^\circ$ suggests that the line-of-sight direction is tilted to nearly perpendicular to the vector pointing from the MBH to the ascending node of the star intersecting with the accretion disk.

The best-fit value deviating slightly from those from the mean likelihood in Table 1 is due to the two local minima of χ^2, as is more clearly shown in Figure 3. The two local minima are more apparent for $M_\bullet$ and $a_\bullet$, where one of them is the best-fit value at $M_\bullet = 2.69 \times 10^5\, M_\odot$ and $a_\bullet = 390 r_g$ (marked by the yellow cross), and the other is at $M_\bullet \sim 3.8 \times 10^5\, M_\odot$ and $a_\bullet \sim 320 r_g$. As the size of the MCMC chains is sufficiently large ($\sim 10^5$ accepted MC samples), the two local minima are more likely due to the fluctuations caused by the small sample size of the QPE or some unknown systematics in the data.

Comparison of the observed QPEs of GSN069 and the TOA of each eruption in the best-fit model are shown in Figure 2 (marked by red arrows). The TOAs of each QPE from observations are well consistent with those from simulations within 2σ errors.

The time intervals between QPEs in each observation are more clearly presented in Figure 4. It is interesting to see that the TOA of both the observed and simulated QPEs are with alternate short and long intervals, which irregularly vary by the amount of 2–3 ks. Such quasi-periodic behavior can be explained by combination effects of the Schwarzschild precession and the presence of a small eccentricity of the orbit of the star. The time interval between QPEs should be in orders of $P_{1/2} + \delta P(f_0)$, where $P_{1/2}$ is the half-orbital period, and $\delta P(f_0) \sim 4e \sin f_0/\dot{\omega}_\bullet = 4e \sin f_0 (M_\bullet G)^{-1/2} a_\bullet^{3/2}$ (when $e_\bullet \ll 1$), where $\dot{\omega}_\bullet = (GM_\bullet/a_\bullet^3)^{1/2}$ is the orbital angular velocity and f_0 is the true anomaly of the orbiter when it hits on the disk. If there is no orbital precession (f_0 = constant), the time interval should be either $P_{1/2} + \delta P(f_0)$ or $P_{1/2} + \delta P(f_0 + \pi) = P_{1/2} - \delta P(f_0)$. Due to Schwarzschild and Lense–Thirring orbital precession, f_0 precesses in each orbit and the interval of QPEs will be modulated between $P_{1/2} + \delta P(\pi/2)$ and $P_{1/2} - \delta P(\pi/2)$. For GSN069, we find that $\delta P(\pi/2) \sim 2.4$ ks, which is consistent with those shown in the right panel of Figure 4. In a Schwarzschild black hole, the orbital precession become 2π after a total of $N_{\mathrm{p,\,S}}$ flares, which is

$$N_{\mathrm{p,\,S}} = \frac{4\pi}{\delta\omega_{\mathrm{S}}} = \frac{2a_\bullet}{3r_g}(1 - e_\bullet^2) \simeq 259, \quad (3)$$

where $\delta\omega_{\mathrm{S}} = 6\pi(a_\bullet/r_g)^{-1}(1 - e_\bullet^2)^{-1}$. This is also consistent with the period of modulation $N_{\mathrm{p,\,S}} \sim 258$ shown in the right panel of Figure 4. The difference of time per flare is then approximately $2\delta P(\pi/2)/N_{\mathrm{p,\,S}} \propto a_\bullet^{1/2}$,[6] thus the larger the distance of the orbiter, the larger the relativistic effects on TOA of QPEs around a Schwarzchild MBH.

In summary, we find that the observed TOA of the QPEs of GSN069 can be well explained by the star–disk collision models and some of the parameters of the orbit of the star can be well constrained by using only the timing of the X-ray emission of QPEs. The quasi-periodic behavior can be explained by combination effects of a small orbital eccentricity of the orbiter and the Schwarzschild precession.

4. Is the Orbiter in GSN069 a Stellar Core from a Previous Partial TDE?

Recent observations suggest that GSN069 exhibits some characteristic of a partial TDE (Sheng et al. 2021; Zhao et al. 2021). Considering that the QPEs of GSN069 exhibit long-lived signatures of a TDE (Shu et al. 2018), here we show that, if the star–disk collision model is the driving mechanism of QPEs of GSN069, the orbiter may be a stellar core remaining after a partial tidal disruption of an evolved star (possibly a red giant) around the MBH in GSN069. More details are provided as follows.

Partial TDEs can happen if a red giant star passes through the MBH near the tidal radius $r_p \sim r_t = r_\star (M_\bullet/m_\star)^{1/3}$, where $r_\star$ and $m_\star$ are the radius and the mass of the red giant, respectively (e.g., MacLeod et al. 2012; Bogdanović et al. 2014; Coughlin & Nixon 2019; Chen & Shen 2021). Typically for a red giant $r_\star = 5 \sim 20\, R_\odot$ when $m_\star \sim 1$–$5\, M_\odot$ (MacLeod et al. 2012). As the stellar core is more compact than the outer envelope, the stellar core remained while the envelope was disrupted by the tidal force of the MBH. Then the stellar core

[6] See similar "sidereal period" in the case of Schwarzchild, Lense–Thirring, and quadruple momentum orbital precession in Iorio (2016) and Iorio & Zhang (2017).

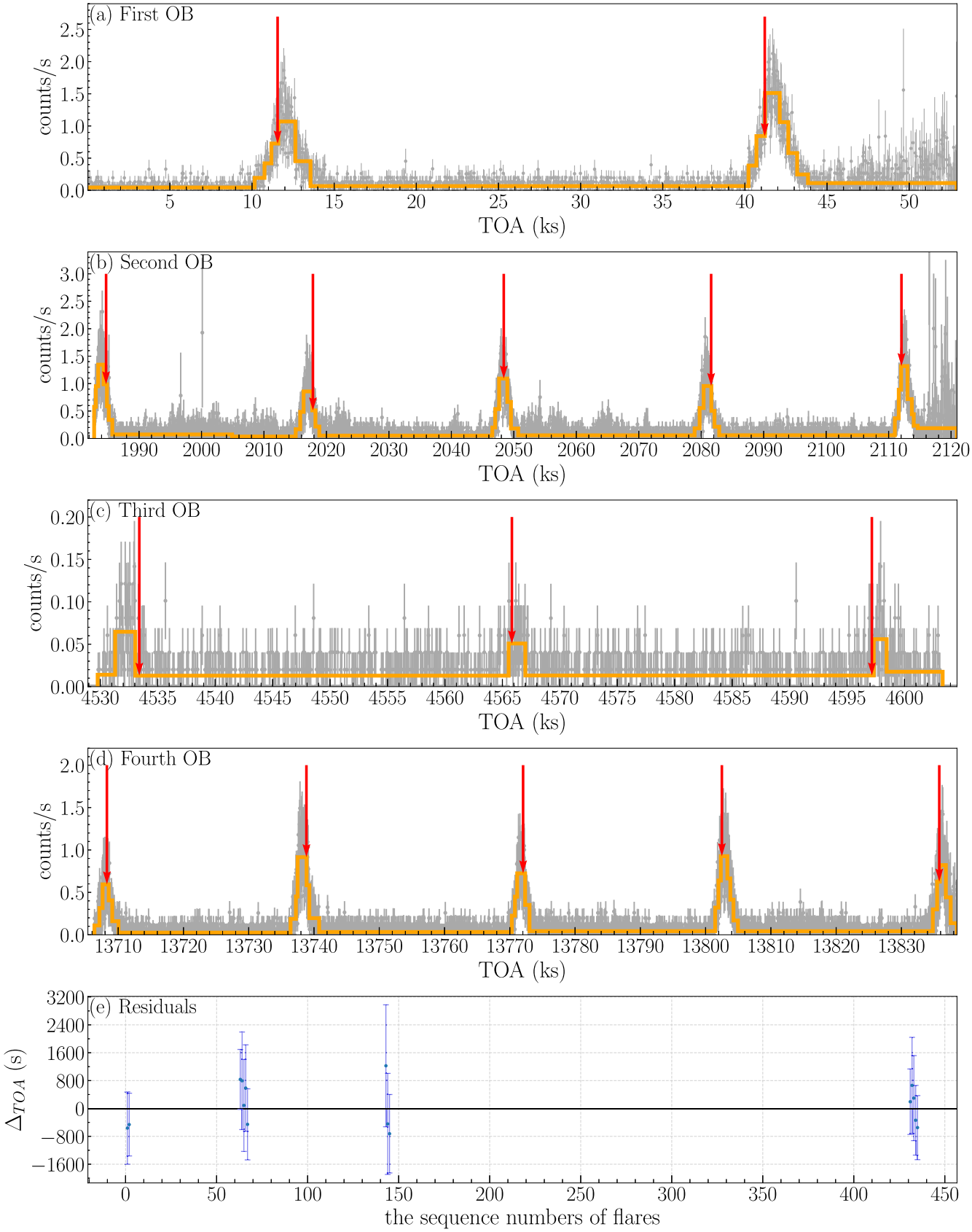

Figure 2. Panels (a)–(d): the observed X-ray flux of QPEs in GSN069 (Miniutti et al. 2019) from 2018 December to 2019 May (gray dots with error bar) and the TOA of QPEs from the best-fit models (marked by the red arrows). The orange solid lines show the optimal Bayesian block representations near each eruption. Panel (e) shows the residual of the TOA between the model and the observation, where the error bars show the 2σ uncertainty of the TOA. The horizontal axis of panel (e) shows the number of sequences of each eruption from the modeling.

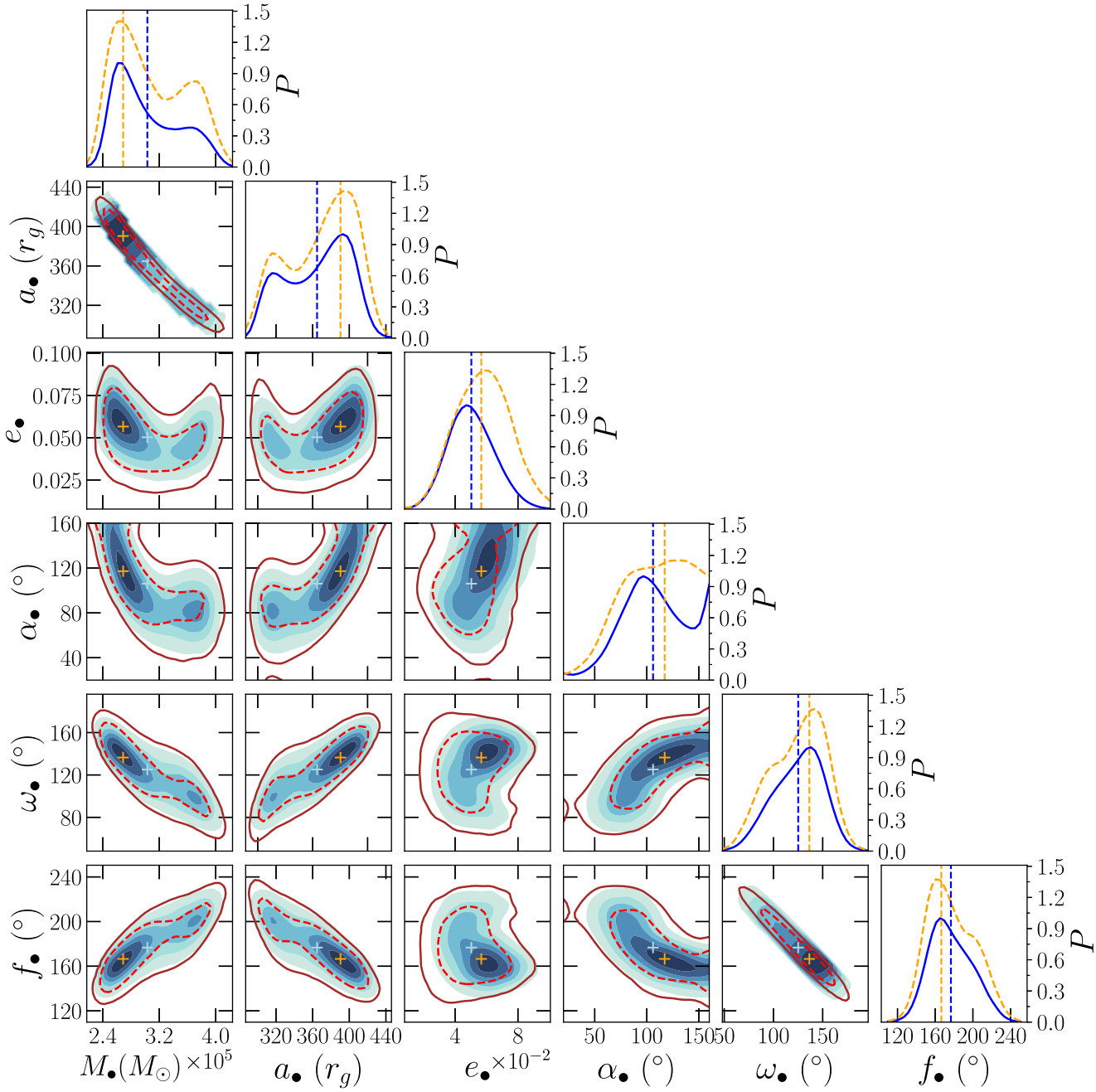

Figure 3. The reconstructed initial orbital elements of the orbiter by using the X-ray timing of GSN069. The color contour maps represent the mean likelihood of the MCMC sample, and the line contours represent the marginalized distribution, with the 1σ (dashed line) and 2σ (solid line) confidence levels. The panels in triangle show the one-dimensional probability distribution. The mean-likelihood value and those with minimum χ^2 of each parameter are marked by the light-blue and yellow crosses in each panel, respectively.

should be initially with orbital periapsis $r_p \sim 300$–$2075\ r_g$ for GSN069 with $M_\bullet \sim 3\times10^5\,M_\odot$. This result is consistent with the distance of $\sim$400r_g of the orbiter from the MBH for GSN069 resulting from our constraints. Note that the above estimation is for initial value of r_p and the orbit of the stellar core may evolve later due to the collisions with the accretion disk (see later in the text).

During each collision, part of the kinematic energy of the star is transferred into the shocked gas. As the radius of the remnant core is usually $r_{\rm core} \sim r_\star/20 \sim 0.1R_\odot$ (MacLeod et al. 2012), the X-ray luminosity of the eruption is then given by

$$L_X \sim 10^{43}\,{\rm erg/s}\,f_X\,\frac{\epsilon^2}{\lambda^2}\left(\frac{r_{\rm core}}{0.1\,R_\odot}\right)^2\frac{0.01}{\alpha}\left(\frac{M_\bullet}{10^6\,M_\odot}\right)^{-1}, \quad (4)$$

where f_X is the fraction of emission in X-ray that depends on the details of radiative processes (Nayakshin et al. 2004) and $r_{\rm core}$, α, ϵ, and λ are the radius of the stellar core, viscosity, radiative efficiency, and Eddington ratio of the disk, respectively. The typical X-ray luminosity of QPEs are in orders of $10^{41}\sim10^{42}$ erg s^{-1} (Miniutti et al. 2019; Arcodia et al. 2021); thus, the above estimation is consistent with the observed luminosity when $f_X \sim 0.01$–0.1.

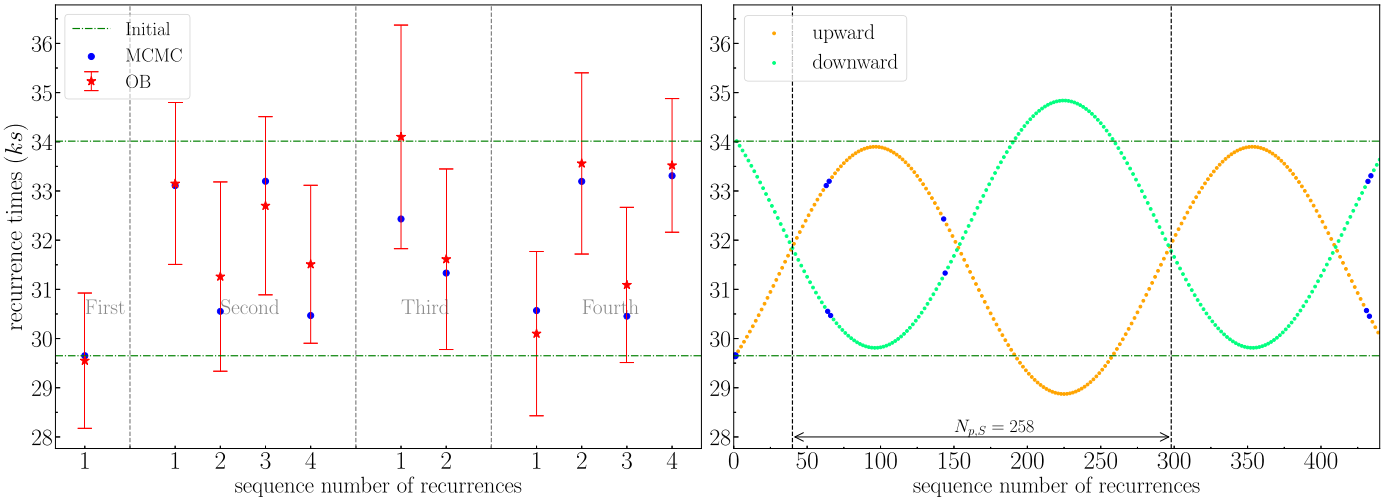

Figure 4. The time interval between flares in each period of observation. Left panel: data marked by the red star and the blue dot represent the observation of GSN069 and the corresponding best-fit results in the MCMC modeling, respectively. The error bars show the 2σ error of the uncertainties in TOA. The dashed–dotted dark green lines (34.01 ks and 29.65 ks) show the expected time interval in the Newtonian case. Right panel: time interval between QPEs for the best-fit model for a total of 450 flares. Green (yellow) dots show the interval between the moment that the orbiter crosses the disk upward (downward) and then downward (upward).

Table 1
Orbital Elements Reconstructed from QPEs in GSN069

Parameters	Range[a]	Constraints[b]	Best Fit[c]
$P_k[ks]$	$(0\ 10^4)$	$64.222^{+0.105}_{-0.073}$	64.180
$M_\bullet[M_\odot]$	$(0\ 3\times10^8)$	$3.03^{+0.92}_{-0.61} \times 10^5$	2.69×10^5
$a_\bullet[r_g]$	(100 700)	$364.8^{+54.0}_{-49.0}$	390.4
$e_\bullet$	(0 1)	$0.050^{+0.030}_{-0.026}$	0.057
$\alpha_\bullet[°]$	(20 160)[d]	$106.0^{+54.0}_{-49.0}$	117.1
$\omega_\bullet[°]$	(0 360)	$125.1^{+42.5}_{-50.6}$	136.4
$f_\bullet[°]$	(0 360)	$176.7^{+45.9}_{-38.8}$	166.5

Notes.
[a] The prior ranges for parameters.
[b] The constraints of parameters from mean likelihood in the 2σ confidence level.
[c] The parameters with minimum χ^2 value ($\chi^2 = 16.2$).
[d] Here $\alpha_\bullet$ should avoid an angle near 0° or 180° where the disk is edge-on, which can cause difficulties in the light-tracing numerical methods.

The star will experience drag force caused by sweeping up of the intercepted disk gas in each collision, and finally the orbit is circularized and aligned with the disk. Following Rauch (1995), the alignment timescale ($t_{\rm align}$) is assumed to be approximately the time needed for a star to intercept with the disk material with masses equal to its own masses, which is given by[7]

$$\frac{t_{\rm align}}{t_{\rm orb}} \sim 1.3 \times 10^6 \frac{m_{\rm core}}{0.1\ M_\odot}\left(\frac{r_{\rm core}}{0.1\ R_\odot}\right)^{-2}\left(\frac{\alpha}{0.01}\right) \times \left(\frac{\lambda}{\epsilon}\right)\left(\frac{a_\bullet}{10^2\ r_{\rm g}}\right)^{-3/2}, \quad (5)$$

where $t_{\rm orb}$ is the orbital period and $m_{\rm core} \sim 0.3$–$0.6\ M_\odot$ (MacLeod et al. 2012) is the mass of the stellar core to the MBH, respectively. For GSN069 with $M_\bullet \sim 3 \times 10^5\ M_\odot$ and $a_\bullet \sim 400 r_g$ (as shown in Section 3), it is then suggested that the QPEs can last for about ~1170 yr. The corresponding gravitational-wave orbital decay is with a timescale of $\geqslant 2 \times 10^6$ yr if $e \leqslant 0.6$ and $m_{\rm core} \sim 0.3\ M_\odot$. As the observation time of QPEs is typically in about $\lesssim$1 yr, it is justified that in our simulations we ignore the changes of the orbit due to both the star–disk collision and the gravitational-wave orbital decay.

As QPE sources are assumed results of partial TDE events, the event rate of QPE sources ($R_{\rm QPE}$) is expected to be the same as those of partial TDE ($R_{\rm pTDE}$), the latter of which are expected to be about 10% of those of normal TDE (disrupting a main-sequence star), i.e., $R_{\rm pTDE} \sim 0.1 R_{\rm TDE} \sim 10^{-5}$ yr^{-1} per galaxy (with $M_\bullet < 10^7\ M_\odot$; MacLeod et al. 2012). As the duration of QPE events can be $T_{\rm QPE} \sim 1000$ yr, the duty cycle of QPE sources is then expected to be around $R_{\rm QPE} T_{\rm QPE} \sim 10^{-2}$, suggesting that QPEs may appear in every 1 of 100 late-type galaxies (with $M_\bullet < 10^7\ M_\odot$) at any given moment. It will be easier to understand the frequency of QPE sources if we obtain the number ratio between the QPE sources and those of normal TDE:

$$\mathscr{R} = \frac{R_{\rm QPE}}{R_{\rm TDE}} \times \frac{T_{\rm QPE}}{T_{\rm TDE}} \sim 10^2\text{–}10^3, \quad (6)$$

where $T_{\rm TDE} \sim 0.1$–1 yr is the duration of normal TDE events. The above estimation suggest that theoretically the QPE sources should be much more abundant than those of normal TDE sources. Currently there are only a few QPE sources revealed, possibly because the observation of them is quite expensive, and that not all of them produce bright enough flares.

5. Constraining the Spin Parameters of the MBH by TOA of QPEs

The TOA of QPEs also can be affected by the presence of the spinning of the MBH due to Lense–Thirring effects on the orbit and the additional deflection of lights by the frame-dragging effects. We investigate the constraints on the spin

[7] Note that orbital eccentricity and inclination respect to the disk plane can also affect the alignment timescale (for more details see Vokrouhlicky & Karas 1993; Rauch 1995). If initially the orbital inclination is low, the eccentricity will stay at a low eccentric value for a long time (Rauch 1995). Thus, the probability of observing a GSN069-like system with a low eccentric value of the orbiter (~0.06) will be higher if initially the orbital inclination is low.

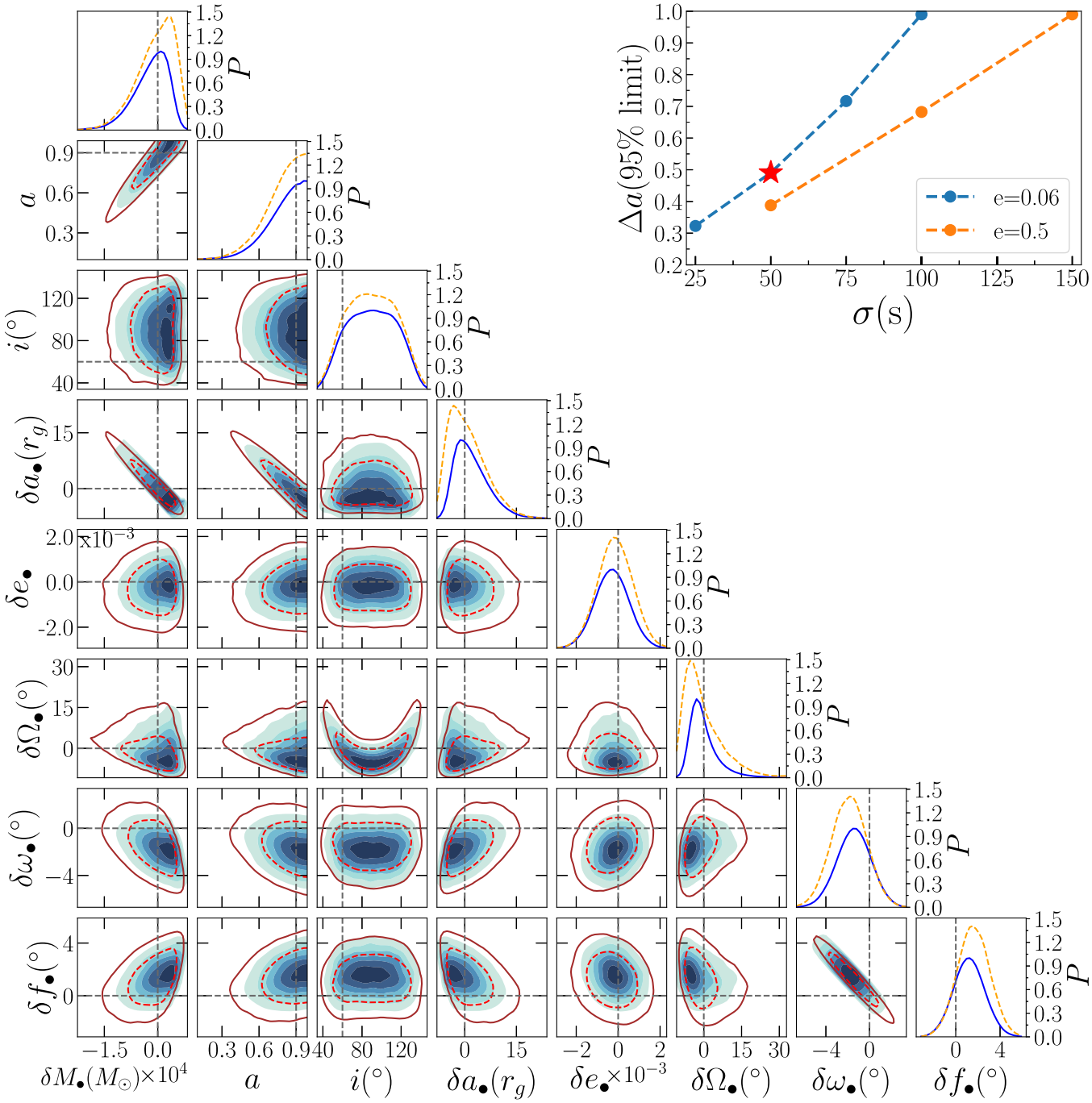

Figure 5. Top right panel: constraints on the amplitude of spin a in the case of different orbital eccentricities, or the assumed timing measurement errors of the TOA of QPEs for a GSN069-like MBH.Twenty-five of 425 QPEs are used for MCMC, corresponding to a duration of about ∼155 days. Panels on the left: The constraints on the parameters in the cases $\sigma_t = 50$s and $e_\bullet = 0.06$ (corresponding to the red star symbol in the top right panel). The contours and the marginalized probabilities are similar to those in Figure 3. $\delta M_\bullet$, $\delta a_\bullet$, $\delta e_\bullet$, $\delta\Omega_\bullet$, $\delta\omega_\bullet$, and $\delta f_\bullet$ show the difference with respect to the input value of the mock data. The dashed line in each panel shows the position of the input value.

parameters of the MBH (also other model parameters simultaneously) by using mock observations, which corresponds to those that can possibly be collected in the near future for QPE sources. We find that the inclination $I_\bullet$ has a near-degeneracy with the spin parameter a, which largely slows down the convergence of the MCMC simulations. As usually $I_\bullet$ can only be poorly constrained, here we fix $I_\bullet$ for simplicity. If $I_\bullet$ is taken as a free parameter, we find that our following constraints on a are only slightly weaker (e.g., an increase from $\Delta a \sim 0.5$ to $\Delta a \sim 0.6$).

For demonstration purposes, we choose QPEs from a GSN069-like galaxy given the best-fit values suggested by Table 1: $M_\bullet = 2.65 \times 10^5 M_\odot$ (or $P_k = 63.16$ ks), $a = 0.9$, $i = 60°$, $a_\bullet = 390 r_g$, $e_\bullet = 0.06$ or 0.5, $I_\bullet = 45°$, $\Omega_\bullet = 120°$, $\omega_\bullet = 140°$, and $f_\bullet = 160°$. There are a total of eight free parameters in the MCMC: (P_k, a, i, $a_\bullet$, $e_\bullet$, $\Omega_\bullet$, $\omega_\bullet$, and $f_\bullet$). We simulate a total of 425 flares, which corresponds to a time duration of ∼155 days. To mimic the intermittent observation, only the 1st–5th, 106th–111th, ..., and 421st–425th eruptions (a total of 25 eruptions) are used for recovering.

By performing a number of MCMC simulations, we explore the constraints on the spin magnitude in case of different timing measurement uncertainties or the orbital eccentricities. The results are shown in Figure 5. In the case when $e_\bullet = 0.06$, the constraints of spin are only possible if $\sigma_t \lesssim 100$ s. However, if $e_\bullet = 0.5$, the constraints can be stronger and the spin parameter can be revealed if $\sigma_t \leqslant 150$ s. The results of the reconstructed model parameters are also shown in the left panels in Figure 5 given the uncertainties of TOA $\sigma_t = 50$ s and $e_\bullet = 0.06$. We can see that both the orbital elements and the spin of MBH can be recovered, where the uncertainties of $\Delta a \sim 0.49$ and $\Delta i \sim 85°$, respectively.

In principle, orbiters similar to the above one but with higher eccentricities, or QPE observations covering a longer time span, can set even stronger constraints on the spinning of the MBH. By methods similar to those in Section 3, we expect that the time difference per flare due to the Lense–Thirring effect is approximately $2\delta P(\pi/2)/N_{\rm p,L}$, where $N_{\rm p,L} = 4\pi/|\delta\omega_L|$, and $|\delta\omega_L| = 12\pi a(a_\bullet/r_g)^{3/2}(1-e_\bullet^2)^{-3/2}\cos I_\bullet$. Note that $2\delta P(\pi/2)/N_{\rm p,L}$ is independent of $a_\bullet$. Similarly, the variations due to quadruple momentum effects $2\delta P(\pi/2)/N_{\rm p,\,Q} \propto a_\bullet^{-1/2}$, where $N_{\rm p,\,Q} \propto a_\bullet^{-5/2}$. We defer exploring more details of the constraining of the spin on various conditions of the orbiters by timing of QPEs to future studies.

6. Summary

X-ray quasi-periodic eruptions (QPEs) in active galactic nuclei are found recently with unknown driving mechanisms. By assuming that QPEs are driven by star–disk collisions, we develop a full relativistic model to reconstruct the parameters of the orbiter and also the spinning of the massive black hole (MBH) by using the time of arrival (TOA) of these QPEs.

We apply our method to the QPEs of GSN069, and find that the orbital parameters of the star can be well constrained, although the spinning of the MBH cannot, due to the limited timing accuracy of the observed samples. The orbiter in GSN069 is found with a semimajor axis of about $365^{+54}_{-49} r_{\rm g}$ and a small eccentricity ($e_\bullet = 0.05^{+0.02}_{-0.02}$) around an MBH with $M_\bullet = 3.0^{+0.9}_{-0.6} \times 10^5\, M_\odot$. We find that the variations on the recurring time of QPEs of GSN069, with repeating irregular alternative long and short intervals, can be well explained by the presence of the orbital eccentricity and the relativistic orbital precession. We also discuss the possibilities that the QPEs in GSN069 are caused by continual collisions between a stripped stellar core with the accretion disk around the MBH, the former of which are formed by partial tidal disruption of a red giant.

We find that, for a GSN069-like QPE source that lasts more than several months, if the timing uncertainties of the TOA of QPEs can be less than ∼100–150 s, the spinning of the MBH can be constrained. Orbiters with higher eccentricities, or QPE observations covering a longer time span, can be used to set even stronger constraints on the spinning of MBH.

If the X-ray QPEs are driven by the star–disk collisions around the MBH, the time of arrival of each QPE includes various general relativistic effects around the MBH. Our results suggest that long-time monitoring of X-ray QPEs can provide a unique probe of general relativistic effects, the spinning of MBH, tests of the no-hair theorem, and also gravity theories.

We thank the anonymous referee for the helpful comments that have improved this Letter. This work was supported in part by the Natural Science Foundation of Guangdong Province under grant No. 2021A1515012373, National Natural Science Foundation of China under grant No. 11603083. This work was supported in part by the Key Project of the National Natural Science Foundation of China under grant Nos. 11733010 and 12133004. This work was also supported in part by the Joint Research Foundation in Astronomy (U1731104, U2031106) under cooperative agreement between the NSFC and the CAS, Chinese Science Foundation (NSFC-11833007, 11822301, 11733001), the science research grants from the China Manned Space Project with No. CMS-CSST-2021-B11. The simulations in this work are performed partly in the TianHe II National Supercomputer Center in Guangzhou.

ORCID iDs

Fupeng Zhang https://orcid.org/0000-0002-0403-9522
Liming Dou https://orcid.org/0000-0002-4757-8622
Xinwen Shu https://orcid.org/0000-0002-7020-4290

References

Arcodia, R., Merloni, A., Nandra, K., et al. 2021, Natur, 592, 704
Bogdanović, T., Cheng, R. M., & Amaro-Seoane, P. 2014, ApJ, 788, 99
Chen, J.-H., & Shen, R.-F. 2021, ApJ, 914, 69
Coughlin, E. R., & Nixon, C. J. 2019, ApJL, 883, L17
Coughlin, E. R., & Nixon, C. J. 2020, ApJS, 247, 51
Dai, L. J., Fuerst, S. V., & Blandford, R. 2010, MNRAS, 402, 1614
Gierliński, M., Middleton, M., Ward, M., et al. 2008, Natur, 455, 369
Giustini, M., Miniutti, G., & Saxton, R. D. 2020, A&A, 636, L2
Ingram, A., Motta, S. E., Aigrain, S., & Karastergiou, A. 2021, MNRAS, 503, 1703
Iorio, L. 2016, MNRAS, 460, 2445
Iorio, L., & Zhang, F. 2017, ApJ, 839, 3
Ivanov, P. B., Igumenshchev, I. V., & Novikov, I. D. 1998, ApJ, 507, 131
Karas, V., & Vokrouhlicky, D. 1994, ApJ, 422, 208
King, A. 2020, MNRAS, 493, L120
Lehto, H. J., & Valtonen, M. J. 1996, ApJ, 460, 207
Lightman, A. P., & Eardley, D. M. 1974, ApJL, 187, L1
MacLeod, M., Guillochon, J., & Ramirez-Ruiz, E. 2012, ApJ, 757, 134
Miniutti, G., Saxton, R. D., Giustini, M., et al. 2019, Natur, 573, 381
Nayakshin, S., Cuadra, J., & Sunyaev, R. 2004, A&A, 413, 173
Pasham, D. R., Remillard, R. A., Fragile, P. C., et al. 2019, Sci, 363, 531
Pihajoki, P. 2016, MNRAS, 457, 1145
Raj, A., & Nixon, C. J. 2021, ApJ, 909, 82
Rauch, K. P. 1995, MNRAS, 275, 628
Semerák, O., Karas, V., & de Felice, F. 1999, PASJ, 51, 571
Scargle, J. D., Norris, J. P., Jackson, B., et al. 2013, ApJ, 764, 167
Sheng, Z., Wang, T., Ferland, G., et al. 2021, ApJL, 920, L25
Shu, X. W., Wang, S. S., Dou, L. M., et al. 2018, ApJL, 857, L16
Suková, P., Zajaček, M., Witzany, V., & Karas, V. 2021, ApJ, 917, 43
Valtonen, M. J., Mikkola, S., Lehto, H. J., et al. 2011, ApJ, 742, 22
Valtonen, M. J., Lehto, H. J., Nilsson, K., et al. 2008, Natur, 452, 851
Vaughan, S. 2010, MNRAS, 402, 307
Vokrouhlicky, D., & Karas, V. 1993, MNRAS, 265, 365
Zentsova, A. S. 1983, Ap&SS, 95, 11
Zhang, F., Lu, Y., & Yu, Q. 2015, ApJ, 809, 127
Zhang, F., & Saha, P. 2017, ApJ, 849, 33
Zhao, Z. Y., Wang, Y. Y., Zou, Y. C., et al. 2021, arXiv:2109.03471